Electronic band structure of phosphorus-doped single crystal diamond: Dynamic Jahn-Teller distortion of the tetrahedral donor ground state

V. D. Blank,[1,2] K. N. Boldyrev,[2,3,*] V. N. Denisov,[1,2,3,†] V. V. Denisov,[1] A. S. Galkin,[1,3] M. S. Kuznetsov,[1] B. N. Mavrin,[3,‡] S. A. Nosukhin,[1] D. D. Prikhodko,[1,2] A. A. Sukhanov,[4] S. A. Tarelkin,[1,2] and S. A. Terentiev[1]

[1]*Technological Institute for Superhard and Novel Carbon Materials, 108840 Troitsk, Moscow, Russia*

[2]*Moscow Institute of Physics and Technology, 141700 Moscow Region, Russia*

[3]*Institute of Spectroscopy, Russian Academy of Sciences, 108840 Troitsk, Moscow, Russia*

[4]*Zavoisky Physical-Technical Institute, FRC Kazan Scientific Center of RAS, 420029 Kazan, Russia*

(Received 11 January 2019; revised 21 July 2020; accepted 22 July 2020; published 24 September 2020)

The electronic band structure of the phosphorus-doped high-quality high-pressure and high-temperature–grown single crystal diamond was studied by infrared absorption, magneto- and electron paramagnetic resonance spectroscopy, and first-principles calculations. The complete picture of the $1s \rightarrow np_{\pm}$ and $1s \rightarrow np_0$ ($n = 2, 3, 4$) donor transitions with new $1s \rightarrow 3p_0, 4p_0$ and $1s \rightarrow 4p_{\pm}$ transitions allowed us to refine the energy levels of ground and exited states with those obtained from effective mass approximation calculation. For the first time, as far as we know, we have observed the fine doublet structures of the $1s(B_2, E) \rightarrow 2p_{\pm}$, $1s(B_2, E) \rightarrow 4p_0$, $1s(B_2, E) \rightarrow 3p_{\pm}$, and $1s(B_2, E) \rightarrow 4p_{\pm}$ donor transitions with the splitting value of 1.05 meV. These doublet structures arise from the dynamic Jahn-Teller (JT) distortion which splits the energy level of the $1s(T_2)$ state in the T_d configuration into those of the $1s(B_2)$ ground state and the $1s(E)$ state in the D_{2d} configuration. The dynamic JT distortion of the tetrahedral donor ground state has been proved by following facts: the observation of vibronic energy levels and temperature behavior of doublet bands in the IR spectrum, the absence of P-donor-related electron paramagnetic resonance signals, and first-principles calculations. We believe that the dramatic broadening of the $2p_0$ band attributed to the $1s(B_2, E) \rightarrow 2p_0$ donor transition at 524 meV is caused by the resonant interaction of this 524 meV energy level with that of ~517 meV formed due to the dynamic JT coupling of the $1s(E)$ energy level equal to 387 meV with the longitudinal acoustic phonon of ~130 meV.

DOI: 10.1103/PhysRevB.102.115153

I. INTRODUCTION

Ultrawide-band-gap diamond, with the band gap of 5.47 eV, a breakdown field >10 MV/cm, high electron and hole mobilities >2000 cm^2/V s, and high thermal conductivity of 22 W/cm K, has compelling potential advantages over the most-known analog, such as the narrow-band-gap silicon (Si), in radiation-resistant, high-power, and high-frequency electronics, as well as in deep-UV optoelectronics, quantum information, and extreme-environment applications [1]. The knowledge of the electronic band structure of the phosphorus (P)-doped n-type diamond is important as in solid-state physics as in the development of a quantum computer. Excited states of P-doped diamond, which are close to excited states for deep donor states in silicon doped with S^+ or Se^+ [2,3], as well a spin triplet excited state ^3E of a negatively charged nitrogen-vacancy (NV^-) center in diamond which should experience a dynamic Jahn-Teller effect [4], are promising solid-state qubits for quantum information processing. Deep donors in silicon and the P donors in a diamond can be used for quantum computing, spin-to-photon conversion, photonic memory, integrated single-photon sources, and all-optical switches, because the read-in/read-out is in the optical region showing extremely high decoherence time up to hours [5].

The boron (B) acceptor level of 0.37 eV above the valence band maximum [6] and the P donor level of 0.6 eV below the conduction band minimum [7–10] are formed at the substitutional B or P incorporation into the diamond lattice. Today, the search for other shallow donors in a diamond is still challenging, although two decades have passed since the publication of Kalish's review [11]. These B-acceptor and P-donor levels are relatively deep and only ~0.2% of acceptor holes and ~0.001% of donor electrons are ionized at room temperature, which limits the operation of diamond-based electronic devices. High phosphorus doping of diamond above ~10^{20} cm^{-3} reduces the activation energy up to 0.027 or 0.05 eV [12,13], which may be associated with an appearance of a really shallow donor level. Recently we have found by the observation of the evolution of the $1s(p_{3/2})$, $1s(p_{1/2}) \rightarrow ns(p_{3/2})$, $ns(p_{1/2})$ ($n = 2, 3, 4$) acceptor transitions in the electronic Raman spectra of the boron-doped diamond (BDD) with increasing the boron concentrations from ~4×10^{18} to 2×10^{20} cm^{-3} that a similar reduction of the activation energy was due to the formation of the shallow acceptor level of 0.037 eV [14]. BDD undergoes the Mott transition and becomes metallic at boron concentrations above ~2×10^{20} cm^{-3} when acceptor states merge with the valence band of BDD and acceptor transitions are no longer observed in the electronic Raman spectra [14]. Only one band at ~16 cm^{-1}

*kn.boldyrev@gmail.com
†denisovvn@tisnum.ru
‡Deceased 16 July 2019.

(∼2 meV) assigned by Kim *et al.* to the electronic Raman transition between the $1s(p_{3/2})$ and $1s(p_{1/2})$ spin-orbit split ground states of the boron acceptor was directly observed in electronic Raman spectra of BDD with boron concentrations below $\sim 10^{18}$ cm^{-3} [15]. The indirect evidence of this spin-orbit splitting of the acceptor ground state was also given by infrared absorption (IR) spectroscopy [16,17]. From a comparison of the electric-dipole-allowed acceptor transitions from the ground $1s(p_{3/2})$, $1s(p_{1/2})$ to the excited p states in the infrared absorption spectra of BDD at ∼5 K and ∼80 K, pairs of lines with the 2 meV energy separation between them were identified. The appearance of a new line in each pair of lines at higher temperature was attributed to the thermal population of the $1s(p_{1/2})$ ground state lying 2 meV above the $1s(p_{3/2})$ lowest ground state. The question arises whether there is the energy level splitting of the phosphorus donor ground state in the P-doped diamond and what is its possible origin.

The electronic band structure of the P donor states in silicon (a structural analog of a diamond), well studied and documented [18–20], was used for comparison with that in a diamond. In P-doped silicon, donor states exhibit a sixfold degeneracy which is removed by the valley-orbit interaction, forming a singlet $1s(A_1)$ level in the ground state, as well as a triplet $1s(T_2)$ and a doublet $1s(E)$ levels lying upper a $1s(A_1)$ level under the assumption of T_d symmetry of the defect. This was confirmed by the observation of the $1s(A_1) \rightarrow np_0$ and $1s(A_1) \rightarrow np_\pm$ ($n = 2, 3, 4, 5, 6$) donor transitions in IR absorption spectra [20]. For excited p states with magnetic quantum number m, the levels split into a singlet p_0 with $m = 0$ and a doublet $p_\pm$ with $m = \pm 1$. To date, the donor ground-state symmetry of the substitutional P atom in a P-doped diamond is a question of contention. From theoretical models, some studies predict its tetrahedral symmetry T_d and a ground state T_2, when the substitutional P remains on site [21–23], while others support a distortion from T_d symmetry to trigonal C_{2v}, C_{3v} or tetragonal D_{2d} symmetries when the substitutional P displaces away from a tetrahedral site [24–27]. In the case of T_d symmetry of phosphorus, the valley-orbit interaction split the sixfold degenerated donor states into the $1s(T_2)$ ground state and the $1s(E)$, $1s(A_1)$ excited states with the energy levels of 0.62, 0.45, and 0.40 eV relative to the conduction band minimum, respectively [28]. Such order of energy levels, inverted from the normal order in the P-doped silicon, was also observed in the lithium-doped silicon [20,29,30].

Following the Jahn-Teller (JT) effect, also referred to as the JT distortion, in which states that a degenerate electronic ground state undergoes a geometrical distortion removing this degeneracy, the triply degenerate T_2 donor level splits into A_1, E or B_2, E states for C_{3v} and D_{2d} point groups, correspondingly [27]. In the case of the static JT effect, a substitutional impurity atom is sufficiently strong displaced from a tetrahedral site the system undergoes a static distortion to a new configuration of minimum energy which does not have enough to cross the barrier toward another minimum. The typical magnitudes of the displacement and the barrier are ∼0.02 Å and tens of meV, respectively [27,28]. For example, the *P1* substitutional nitrogen center in diamond shows a static trigonal JT distortion from T_d to C_{3v} symmetry confirmed by electron paramagnetic resonance (EPR) [31,32] and by electron-nuclear double resonance (ENDOR) [33]. In the case of the dynamic JT effect a displacement of a substitutional atom and the energy barrier separating equivalent minima are very small, no static distortion occurs, but the system exhibits a coupled motion of the electrons and the vibrational modes so that vibronic wave functions display symmetry of the undistorted system. It was shown by Ham [34] that the dynamic JT effect in a solid-state system having orbital degeneracy may partially quench the spin-orbit interaction, the orbital parts of the Zeeman and hyperfine interactions, and other orbital operators governing response to perturbations such as strain or applied electric fields. Many types of vibronic phenomena observed in a diamond were reviewed by Davies [35]. It was concluded that the JT distortions at trigonal, tetragonal, and tetrahedral defect centers, excluding substitutional nitrogen, are dynamic. The JT effect can be manifested in infrared absorption, photoconductivity, and luminescence spectra by observation splitting of electronic transitions and by an appearance of vibronic energy levels.

Only three transitions $1s \rightarrow 2p_0$, $1s \rightarrow 2p_\pm$, and $1s \rightarrow 3p_\pm$ with energies of 523, 562, and 583 meV, respectively, were early detected in IR absorption of P-doped diamonds [36–40]. These transitions and that of at 575 meV were observed in the photoconductivity experiment [41,42]. The energies of these transitions were in good agreement with those predicted in the effective mass approximation (EMA) for a phosphorus donor [37]. In the photoconductivity spectrum of P-doped diamond an unidentified transition at 544 meV was observed [42], which will further be assigned to a vibronic transition. The attribution of the most intense absorption band to the $1s \rightarrow 2p_\pm$ transition was confirmed by the observation of its splitting into the $1s \rightarrow 2p_+$ and $1s \rightarrow 2p_-$ bands in a magnetic field of 13 T [43]. A full picture of $1s \rightarrow np_0$ and $1s \rightarrow np_\pm$ ($n = 2, 3, 4$) electronic transitions from ground to excited donor states, their possible splitting, and observation of vibronic energy levels would be essential in understanding the phosphorus donor.

The EPR spectroscopy has been used to determine symmetry and a ground state of shallow donors in silicon. Only the symmetric A_1 donor ground state has the nonzero square of the absolute value of the wave function $|\Psi(0)|^2$ and it alone has a hyperfine interaction with the donor nucleus, which is called an isotropic hyperfine splitting. For the doublet E and triplet T_2 donor ground states which have a node at the donor nucleus [$|\Psi(0)|^2 = 0$], no isotropic hyperfine interaction is expected [44,45]. The electron spin resonance measurements determined that the phosphorus donor in silicon exhibits the T_d symmetry with the isotropic ^{31}P hyperfine splitting of 4.2 mT (40 Gs) and the isotropic the Landé splitting factor $g = 1.9985$ [46]. To study P-related defects in diamond many EPR measurements have been performed in samples such as synthetic diamond powder [47], implanted and annealed IIa diamond crystals [51], chemical vapor deposited (CVD) diamond films [45,49,50,52], small single crystals have grown in P-C medium [48,53]. Although in these studies, EPR of P centers were detected, the spin density signals on them had only around 2% [49] or 5% [50] instead of the estimated P concentrations implying that these EPR centers are not P donors [27] but can be associated with P-N complexes or others defect centers. To exclude the effect of diamond substrates and interfaces between them and CVD diamond films on ESR

measurements, single crystal diamonds should be studied. Thus, EPR measurements of the high-quality P-doped single crystal diamond will make it possible to determine symmetry and a donor ground state of the P center.

Theoretical calculations predicted the difficulty to dope P in the diamond lattice due to the high bulk formation energy of P [25,54,55], implying a very low equilibrium solubility of P in bulk diamond. A large enhancement of the P solubility can be reached in tensile strained epitaxial CVD diamond films [25]. This can explain the significant $\sim 10^{20}$ cm^{-3} concentration of P achieved experimentally in the P-doped CVD diamond films [12,13]. An unexpectedly large enhancement of boron solubility in silicon, on the order of 150% for only 1% strain, due to biaxial stress was also predicted [56]. The synthesis of P-doped diamond crystals at high pressure and high temperature (HPHT) in the P-C medium was only realized in two experimental works [57,58], but the physical properties of such crystals were not measured because of their small size. We succeeded to grow the large-sized, high-quality P-doped diamond single crystals by HPHT technique to study their electronic band structure and other physical properties.

In this paper, we report the detail studies of the electronic band structure of the large-sized, high-quality P-doped single crystal diamonds using the high-resolution IR absorption spectroscopy, both at low temperatures and in external magnetic fields, EPR and secondary ion mass spectrometry (SIMS) as well as first-principles calculations.

II. EXPERIMENTAL AND COMPUTATIONAL DETAILES

A. P-doped single crystal diamond growth

Phosphorus-doped diamond single crystals were grown by the temperature gradient method under high-pressure at 5.5 GPa and high temperature at 1440°C in the "toroid" type high-pressure apparatus. Fe-A-C alloy (91:5:4 by wt. %) was used as the solvent metal. Al was added to the solvent as the nitrogen getter. High-purity (99.9995%) graphite was used as the carbon source. Amorphous phosphorus powder was added to the carbon source in a wide range of concentrations as the doping agent. About 0.5–0.6 mm across synthetic diamond crystals with a (100) seed surface were used as the seed material. The temperature in the reaction cell during growth run was directly measured by Pt6%Rh–Pt30%Rh thermocouple with an accuracy ±2°C. An axial temperature gradient between carbon source and seed crystal was estimated as 30°C. A set of the large colorless P-doped diamond single crystals with phosphorus concentrations up to $\sim 10^{17}$ cm^{-3} was grown. The (111) triangular diamond plates with an edge of ∼3 mm and an angle of ∼3° between (111) oriented surfaces with a thickness of 250 microns were cut with a laser from grown crystals and then mechanically polished. The P-doped diamond plates with (111), (110), and (001) surface orientations were prepared for studying possible isotropic and anisotropic contributions in EPR and IR absorption spectra at external magnetic fields.

B. Optical spectroscopy and SIMS

The IR absorption spectra of the P-doped diamond single crystals were measured with Bruker VERTEX 80v and high-resolution Bruker IFS 125 HR vacuum Fourier transform spectrometers. A VERTEX 80v spectrometer recorded infrared absorption spectra in the 1000- to 8000-cm^{-1} spectral region with a spectral resolution of 1 cm^{-1} at temperatures between 80 K and 300 K using a liquid nitrogen cryostat. A globar light source and an MCT detector were used. A Bruker IFS 125 HR spectrometer was used for recording the high-resolution IR absorption spectra from in the 1800- to 8000-cm^{-1} spectral region with spectral resolution up to 0.2 cm^{-1} at temperatures between 5 and 300 K using a closed-circle helium cryostat Cryomech ST-403. A tungsten-halogen light source and an InSb detector were used.

Raman spectra of the P-doped diamond plates were obtained using a homemade multichannel triple-stage spectrometer (a 0.5 m focal length double subtractive monochromator and a 1.2 m focal length spectrometer) with the 0.6 cm^{-1} spectral resolution to estimate their crystalline quality. The 1332.5-cm^{-1} Raman peak with the full width at half maximum (FWHM) of ∼1.7 cm^{-1} almost the same as that observed from the unstressed IIa type diamond indicates the absence of strain in P-doped diamond plates. No defect induced bands in Raman spectra of P-doped diamonds were observed in comparison with those of the boron-doped diamonds [14].

SIMS with a Cameca IMS 4f instrument was used to measure the concentration of P atoms both in-depth and lateral distribution into the P-doped monocrystalline diamond plates. Measurements of several SIMS craters ∼5 microns deep in different places of both surfaces of plates shown that the inhomogeneity of phosphorus concentration in them did not exceed 10%. This allowed us to correctly comparing infrared absorption and SIMS data and using the absorption coefficient of ∼12.3 cm^{-1} at 2000 cm^{-1} corresponding to the two-phonon diamond absorption band for the phosphorus concentration calibration. To quantify measurements of phosphorus concentration the implanted standard with the definite number of phosphorus atoms was used. In this work we have studied two sets of single crystal diamond plates with (111), (110), and (001) surface orientations P-doped to concentrations of $\sim 6 \times 10^{16}$ cm^{-3} and $\sim 1.1 \times 10^{17}$ cm^{-3} measured with the uncertainty of 10%.

C. EPR and magnetospectroscopy

EPR measurements were carried out using an X-band EPR Bruker Elexsys E–680X spectrometer with the dielectric ring resonator ER4118X–MD5–W1. The spectrometer was equipped with a helium flow cryostat by Oxford Instruments for measurements in the temperature region from 4 to 300 K. EPR measurements were performed at the temperatures of 5 K and 300 K.

The experimental setup for magnetospectroscopy is based on Quantum Design Evercool II closed-cycle helium cryostat equipped with a superconductive magnet. Infrared radiation from a Simex FT–801 Fourier transform infrared spectrometer is directed through a fiber-optic probe to samples placed in a Quantum Design cryostat. The sample is mounted on the bottom of the probe. An MCT detector is mounted on the same probe right after the sample. The amplified electric signal from the detector is lead back to the spectrometer. The spectrometer is equipped with a Globar light source and

provides spectral resolution up to 0.5 cm^{-1}. The setup allows us to study IR absorption spectra in the temperature range of 2–77 K and in magnetic fields up to 9 T.

D. Theoretical background

First-principles calculations of the dispersion of the electronic bands, the partial density of the electronic states and the valley-orbit splitting of the donor ground state of the P-doped diamond were carried out in density-functional theory (DFT) approximations. Previously, the DFT method was used to calculate the position of the donor level of phosphorus in diamond, using the formation energy and the marker method [59–61], to find symmetry and structure of the defect [28], and the total density of electronic states [62]. We used the software package CRYSTAL14 [63] and the Heyd-Scuseria-Ernzerhof hybrid functional HSE06 [64]. The basic functions were taken from the site of the package. A supercell approach was used to simulate the doping by the P atom. Although an undoped diamond has a face-centered cubic (FCC) lattice, its doping by the P atom reduces the symmetry of the supercell to hexagonal. A supercell was chosen from 192 atoms, created by multiplying a $4 \times 4 \times 2$ optimized 6-atom primitive diamond cell in hexagonal axes (polytype 3C [65]). The band gap E_g for indirect transitions in the undoped C_{192} diamond was 5.46 eV. In the PC_{191} cell, this E_g decreased to 5.3 eV but remained at the same values of the wave vector as in C_{192}. Parameters of the supercell: a = b = 10.0289 Å, c = 12.2825 Å. In a supercell, one carbon atom was replaced by a P atom. The positions of the atoms were optimized with residual forces between atoms of less than 10^{-2} eV/Å. The supercell parameters remained fixed. The optimization was carried out with integration over the Brillouin zone, using a $2 \times 2 \times 2$ grid for wave vectors. It is known [66] that in the cubic diamond cell the maximum of the valence band is at the Δ_{FCC} point, and the minimum of the conduction band lies along the Δ_{FCC} line (direction Γ_{FCC}–X_{FCC} in the cubic Brillouin zone). When choosing a hexagonal diamond cell, the Δ_{FCC} line is projected in the direction P1-P2 in the hexagonal Brillouin zone [67] [Fig. 1(a), insert].

The coordinates of the points in this direction are P1 (1/2, 0, 1/3) and P2 (0, 0, 5/6). Point P1 corresponds to point X_{FCC} and point P2 (like point Γ) to point Γ_{FCC}. To investigate the dispersion of the electronic bands near the minimum of the conduction band, we have included, in addition to the symmetrical directions of the hexagonal zone, also the direction P1-P2 in the calculations. It turned out that the minimum of the conduction band, as in the undoped diamond, was near point P1 in the direction P1-P2. Additional P branches appear below the carbon branches in the band structure of PC_{191} [Fig. 1(a), color lines]. The partial densities of the electron states for the P and C atoms in the PC_{191} cell are shown in Fig. 1(b). We found that the lowest P branch is associated with the $1s(T_2)$ donor ground state under the assumption of the T_d symmetry of phosphorus. The calculated energy levels of 0.60 and 0.40, 0.36 eV corresponding to the $1s(T_2)$ ground and $1s(E)$, $1s(A_1)$ exited donor states caused by the valley-orbit interaction are close to those in Ref. [28]. Note that the positions of these 1*s* exited phosphorus levels have to be taken with caution because of the 1*s* excited-state properties are beyond the reach of DFT [28].

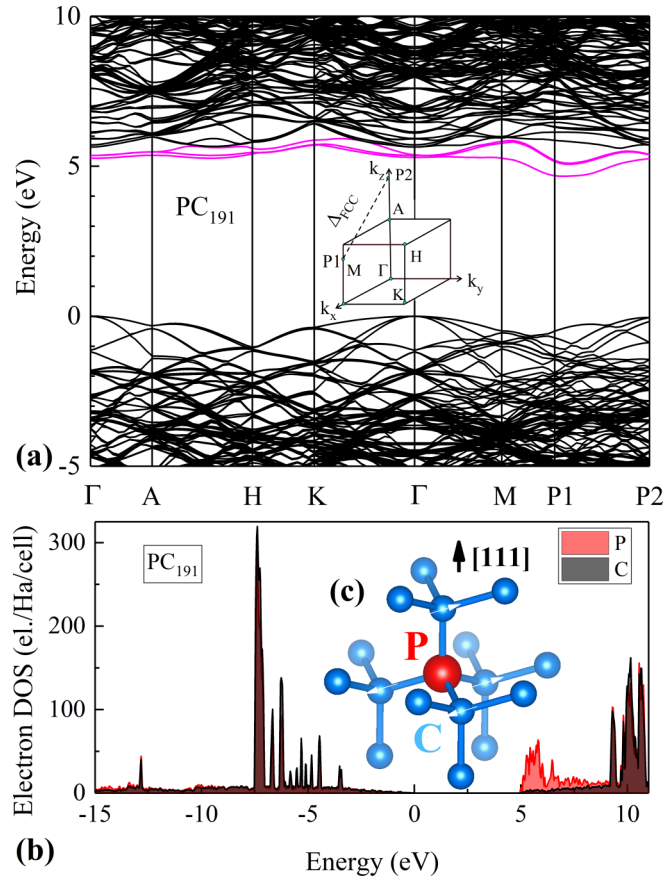

FIG. 1. (a) Dispersion of electronic bands along symmetric directions of the hexagonal Brillouin zone of a P-doped diamond. Insert: Points of the Brillouin zone and the P1-P2 line corresponding to the Δ_{FCC} line in the Brillouin zone. (b) The partial density of the electronic states of phosphorus and carbon atoms in a P-doped diamond. (c) Insert shows the crystal structure of the P center in diamond with Jahn-Teller distortion in the D_{2d} configuration according to Ref. [27].

The static JT distortion caused by the ∼0.02 Å displacement of the substitutional P in diamond will split the triply degenerate $1s(T_2)$ state into the nondegenerate, $1s(B_2)$ ground state and the doubly degenerate $1s(E)$ state in the D_{2d} configuration [28] or into the nondegenerate $1s(A_1)$ ground state and the doubly degenerate $1s(E)$ state in the C_{3v} configuration, similarly to the substitutional nitrogen atom, with the splitting between their energy levels up to ∼100 meV [25,27,28]. If the P atom is displaced from the tetrahedral site T_d to the tetragonal site D_{2d} by only ∼0.002 Å, the value obtained from the DFT calculations, then the system will undergo the dynamic JT distortion. The possibility of a dynamic JT effect when the small amount of the total energy saved by the distortion from T_d to D_{2d} symmetry [Fig. 1(b), insert] was predicted in Ref. [27]. In this case, a small splitting of several meV of bands of electronic transitions and vibronic energy levels can be observed in the IR absorption spectra of the P-doped single crystal diamond.

III. RESULTS AND DISCUSSIONS

Infrared absorption spectra of the high-quality P-doped single crystal diamond plate with the P concentration of $\sim 1.1 \pm 0.1 \times 10^{17}$ cm^{-3} at 90 K and room temperatures are shown in Fig. 2.

The intrinsic two-phonon and three-phonon lattice diamond absorption bands in the range from 1800 to 4000 cm^{-1}, the photoionization continuum from 4000 cm^{-1}, and three bands at 4220, 4540, and 4700 cm^{-1} (523, 562, and 583 meV) attributed to the $1s \rightarrow 2p_0$, $1s \rightarrow 2p_{\pm}$, and $1s \rightarrow 3p_{\pm}$ electronic transitions are observed. The integrated intensity I_{4540} of the band at 4540 cm^{-1} is proportional to the uncompensated donor density, namely N_D-N_A, where N_D and N_A are a donor and compensating acceptor concentrations. The following relation gives the uncompensated donor density measured at 90 K [40]: $N_D - N_A(\text{cm}^{-3}) = (4.2 \pm 0.5) \times 10^{14} \times I_{4540}(\text{cm}^{-2})$. The comparison of the N_D donor concentrations of $\sim 5.5 \pm 0.6 \times 10^{16}$ cm^{-3} and $1.0 \pm 0.1 \times 10^{17}$ cm^{-3} defined from this relation for the P-doped diamond plates with a phosphorus concentration of $\sim 6 \pm 0.6 \times 10^{16}$ cm^{-3} and $\sim 1.1 \pm 0.1 \times 10^{17}$ cm^{-3} measured by SIMS, respectively, shows that at least 90% of phosphorus atoms substitute carbon atoms. The absorption coefficients at the 4540 cm^{-1} peak in infrared spectra at 90 K equal to ~ 8.5 and ~ 5 cm^{-1} for plates with P concentration of $1.0 \pm 0.1 \times 10^{17}$ and $5.5 \pm 0.6 \times 10^{16}$ cm^{-3}, respectively, were found from relation $\alpha = \ln(T)/t$, where T is the normalized sample transmission at 4540 cm^{-1} and $t \approx 250$ microns is the thickness of plates. The absorption coefficient is ~ 12.3 cm^{-1} at the 2000-cm^{-1} peak corresponding to the two-phonon absorption band of the diamond. By comparison the absorption coefficient at the 4540-cm^{-1} peak with that of at the 2000-cm^{-1} peak, one can calibrate the P concentration in the P-doped diamond.

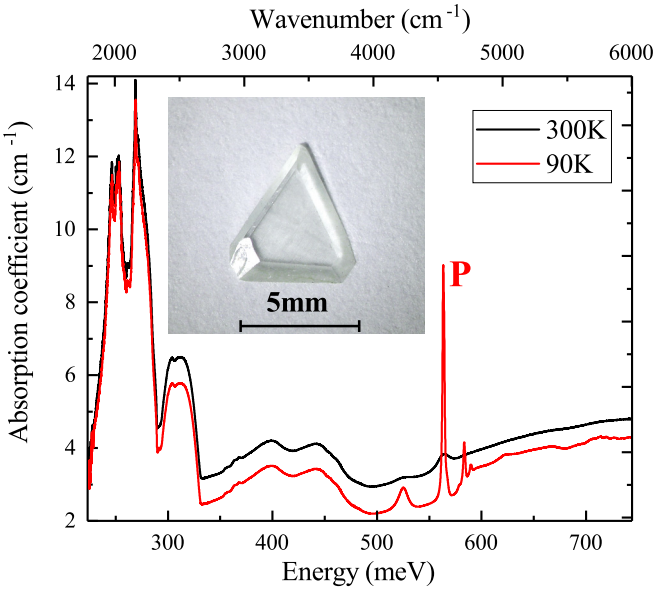

FIG. 2. Infrared absorption spectra of the (111) P-doped single crystal diamond plate at 90 K and room temperatures. Phosphorus concentration measured by SIMS is $\sim 1.1 \pm 0.1 \times 10^{17}$ cm^{-3}. The spectral resolution is 1 cm^{-1}. Insert shows the photo of investigated diamond plate.

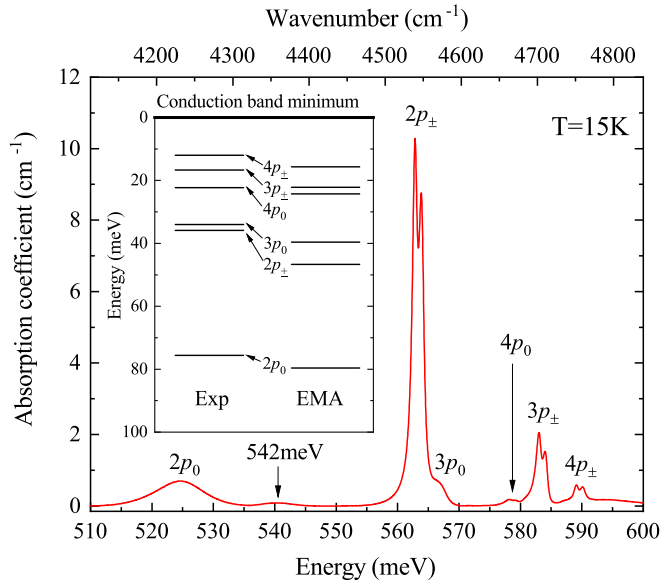

FIG. 3. Absorption coefficient of the (111) P-doped single crystal diamond plate at 15 K. The phosphorus donor concentration is $\sim 1.0 \pm 0.1 \times 10^{17}$ cm^{-3}. The spectral resolution is 0.2 cm^{-1}. The photoionization continuum is subtracted. The insert shows the energy diagram of excited donor phosphorus levels in accordance with experiment and EMA [37]. In this insert, the ground state of $1s$ was assumed to be 600 meV.

The absorption coefficient of the (111) P-doped single crystal diamond plate at 15 K in the energy range from 510 to 600 meV after background subtraction is shown in Fig. 3.

In the IR absorption spectrum obtained with the 0.2-cm^{-1} spectral resolution bands at 524, 564, 566, 578, 583, and 590 meV attributed to corresponding $1s \rightarrow 2p_0$, $1s \rightarrow 2p_{\pm}$, $1s \rightarrow 3p_0$, $1s \rightarrow 4p_0$, $1s \rightarrow 3p_{\pm}$, and $1s \rightarrow 4p_{\pm}$ electronic donor transitions and an unidentified broad band at 542 meV were observed. The insert shows the energy levels diagram of excited donor states in comparison to the experimental data with those calculated by EMA [37]. We found new weak $1s \rightarrow 3p_0$, $1s \rightarrow 4p_0$, and $1s \rightarrow 4p_{\pm}$ donor transitions. The sequence and relative intensity of donor transitions in the IR absorption spectra of the P-doped diamond and the P-doped silicon are very similar. The main difference is the values of the ground-state binding energies of 45.6 and 600 meV for silicon and diamond, the larger spacing between levels in diamond and more narrow line widths in silicon.

For the first time, as far as we know, we have observed the fine doublet structure of the $1s \rightarrow 2p_{\pm}$, $1s \rightarrow 4p_0$, $1s \rightarrow 3p_{\pm}$, and $1s \rightarrow 4p_{\pm}$ donor transitions with the splitting of 8.5 cm^{-1} (1.05 meV) for each doublet. The absence of a doublet structure for the $2p_0$ and $3p_0$ bands is due to strong broadening (FWHM is equal to ~ 8 meV) of the $2p_0$ band and overlapping of $3p_0$ with the intense $2p_{\pm}$ band. We believe that the origin of the fine doublet structure is the dynamic JT distortion of the phosphorus donor with the 1.05-meV energy barrier separating equivalent minima. This distortion caused by the ~ 0.002 Å displacement of P donor from the tetrahedral position to the tetragonal one splits the $1s(T_2)$ ground state in the T_d configuration into the nondegenerate $1s(B_2)$ ground state and the doubly degenerate $1s(E)$ state

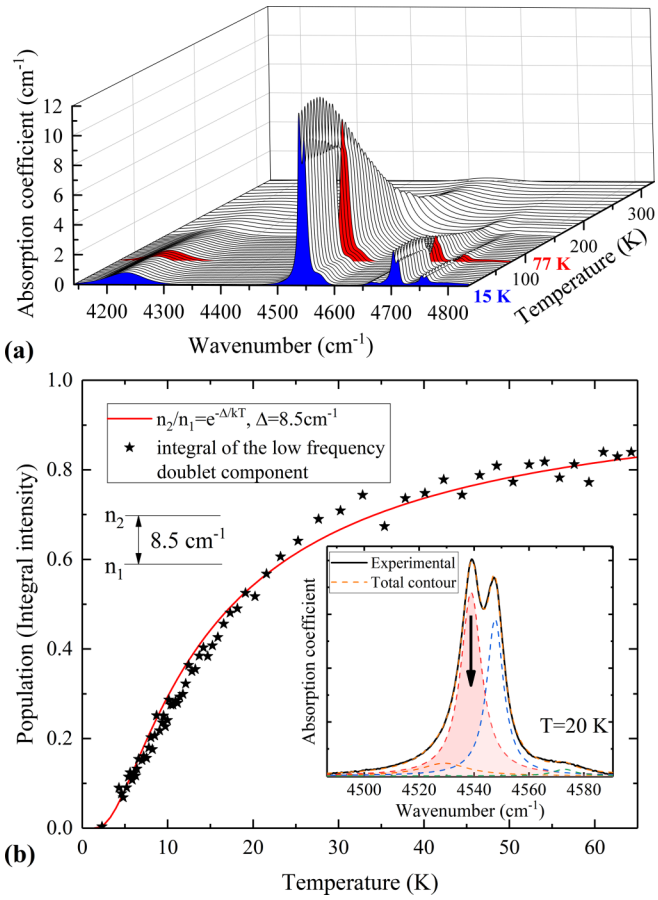

FIG. 4. (a) The evolution of infrared absorption spectra of the (111) P-doped single crystal diamond plate with temperature decreasing from 300 to 15 K. The spectral resolution is 0.2 cm^{-1}. Phosphorus donor concentration, N_D, is $\sim 1.1 \times 10^{17}$ cm^{-3}. (b) The thermal population decrease of the n_2 energy level lying at 8.5 cm^{-1} above the lowest n_1 energy level of the doublet is in accordance to the Boltzmann law.

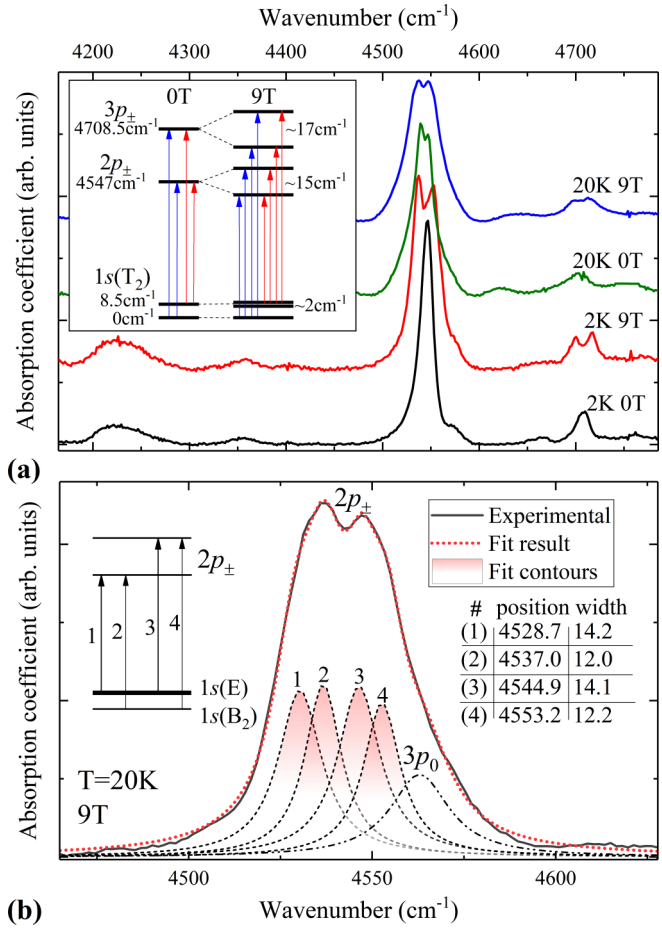

FIG. 5. (a) Infrared absorption spectra of the $1s(B_2, E) \rightarrow np_0$,$np_\pm$ transitions in P-doped diamond at temperatures of 2 and 20 K, and magnetic fields of 0 and 9 T. The insert shows the reconstructed optical transition scheme obtained by dividing bands into Gaussian contours. (b) Contour separation of the $1s(B_2, E) \rightarrow 2p_\pm$ transition in magnetic field 9 T, $T = 20$ K. Left insert: scheme of the observed optical transitions. Right insert: Table with the parameters (position and width in cm^{-1}) of the separated contours.

lying 1.05 meV higher than the $1s(B_2)$ ground state in the D_{2d} configuration. Since there is practically no difference of the P atom positions (on-site or slightly off-site) in the T_d or D_{2d} configurations, we will further adhere to the D_{2d} symmetry of the phosphorus atom with the $1s(B_2)$ ground state and denote the donor transitions with the fine doublet structure as $1s(B_2, E) \rightarrow np_0, np_\pm$ ($n = 2,3,4$).

Another feature of the dynamic JT effect is the appearance in infrared absorption spectra of vibronic energy levels at ~517 meV, causing the strong broadening of the $2p_0$ band at 524 meV, and at 542 meV [see Figs. 3, 5(a), and 6] which are due to the JT coupling of the $1s(E)$ excited states in T_d symmetry with critical points in the continuum of the phonon density of states (PDOS) [34]. The unidentified level at 544 meV was also observed in the Fourier transform photocurrent spectra [42]. Critical points reflect energies of PDOS of the longitudinal acoustic phonon branch (LA) of ~130 meV and the longitudinal optic phonon branch (LO) of 155 meV at L symmetry point near the Brillouin zone boundary [68,69]. We specified the energy level of the $1s(E)$ excited state caused by the valley-orbit interaction in T_d symmetry, equal to 387 meV (the difference between the vibronic energy level of 542 meV and LO of 155 meV) instead of that at 400 meV obtained by us from DFT calculations. The vibronic energy level of ~517 meV [the sum of the $1s(E)$ energy level of 387 meV and LA of ~130 meV] interacts resonantly with the $2p_0$ band of the electronic transition at 524 meV, which causes the dramatic broadening of this $2p_0$ band in IR absorption spectrum. An anomalous broadening of the $1s(A_1) \rightarrow 2p_0$ band of the electronic transition was observed in the IR absorption spectrum of Si-doped with bismuth when the energy of this transition coincided with the optical phonon [70].

The evolution of the IR absorption spectra of the P-doped single crystal diamond plate with temperature decreasing from 300 to 15 K [Fig. 4(a)] was studied to confirm that the electron population of energy levels is governed by Fermi-Dirac statistics. As seen from Fig. 4(a), the intensities of low-frequency components of the doublets decrease with temperature decreasing, while those of the high-frequency components increase. This observation is consistent with the thermal electron population decrease of the $1s(E)$ energy level

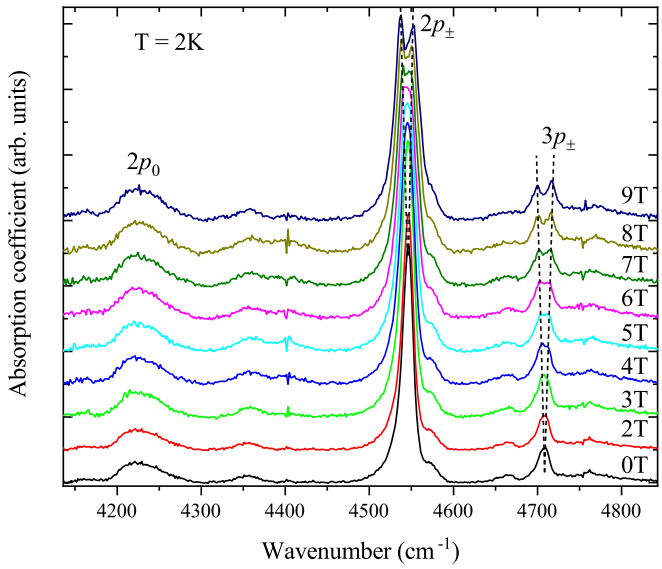

FIG. 6. The evolution of the IR absorption spectra with increasing the magnetic field from 0 to 9 T at the temperature of 2 K.

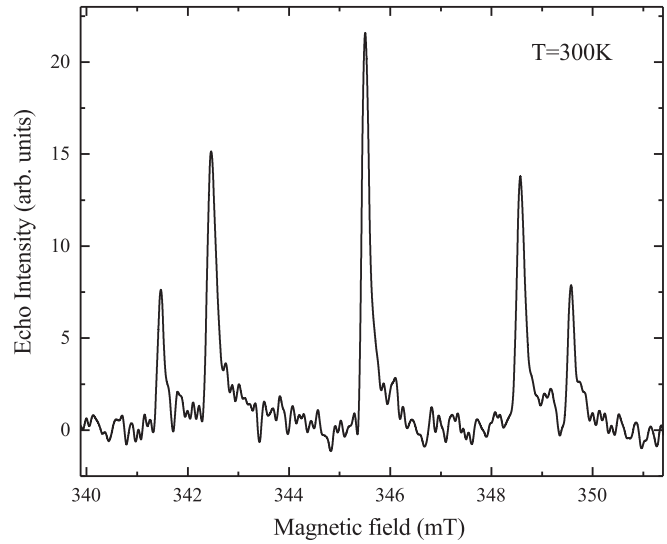

FIG. 7. Echo-detected EPR spectrum at room temperature. The Han pulse sequence was $\pi/2_x$ (16 ns)-τ (300 ns)-π_x (32 ns)-τ-echo.

lying at 8.5 cm^{-1} above the $1s(B_2)$ energy level according to the classical Boltzmann distribution $F(E) \approx e^{-(E-E_F)/k_BT}$ at $E_g \gg E_F$ [Fig. 4(b)]. Our data on the decrease in the intensity of the low-frequency components of the doublets with decreasing temperature unambiguously show that these doublets belong to one P-donor center and not to two centers in different positions.

The IR absorption spectra of the $1s(B_2, E) \rightarrow np_0, np_\pm$ donor transitions in P-doped diamond at temperatures of 2 and 20 K, and magnetic fields of 0 and 9 T are shown in Fig. 5(a) with the reconstructed optical transition scheme obtained by dividing bands into Gaussian contours in the insert.

The infrared absorption spectra of the P-doped diamond plates with (111), (110), and (001) surface orientations were studied both at temperatures of 2 and 20 K and at magnetic fields of 0 and 9 T. The Zeeman splitting of the $1s(B_2)$ ground state in the external magnetic field of 9 T directed parallel to the [111], [110], or [001] axes of the diamond plates with (111), (110), and (001) surface orientations was not found that can be associated with the dynamic JT effect which causes a partial quenching of the orbital part of the Zeeman interaction [34]. In all cases, the same Zeeman splitting of the $2p_\pm$ and $3p_\pm$ bands of ~15 and ~17 cm^{-1} at 9 T was found [Fig. 5(a)].

At the temperature of 2 K only the high-frequency components of the doublet structure of the $1s(B_2, E) \rightarrow 2p_\pm$ and $1s(B_2, E) \rightarrow 3p_\pm$ transitions are observed since the nondegenerate $1s(B_2)$ ground state is ~99.6% populated [see Fig. 5(a), lowest spectrum] in accordance with Boltzmann law that defines the ~1-meV energy barrier separating $1s(B_2)$ and $1s(E)$ minima caused by the dynamic JT distortion of the T_2 ground state in the T_d configuration. A small splitting of ~2 cm^{-1} of the $1s(E)$ state and its absence for the $1s(B_2)$ ground state is evident from the decomposition of the contour into components [see Fig. 5(b)]. Low-energy components from the ground-state doublet [1–3 at Fig. 5(b)] are ~2 cm^{-1} wider than high-energy components [2–4 at Fig. 5(b)]. The evolution of the IR absorption spectra with increasing the magnetic field from 0 to 9 T at the temperature of 2 K is shown in Fig. 6.

Several P-doped diamond single crystals plates with (111), (110), and (001) surface orientations were investigated by the EPR spectroscopy. In the echo-detected EPR spectrum at room temperature, a low-intensity spectrum of the P1 center, arising from single substitutional nitrogen [32], is observed (Fig. 7). Observation of this spectrum was possible only using the spin-echo method with integration over the magnetic field. This is due to the low concentration of this center (less than ~10^{14} cm^{-3}) and the rather long spin-lattice relaxation time, which did not allow the use of the stationary EPR technique. At a temperature of 5 K, the time of spin-lattice relaxation of this center increases significantly and the observation of the spectrum from this center becomes impossible. The appearance of additional spectra associated with P donor centers at the temperature of 5 K was not observed. This fact can be associated with the dynamic JT effect which causes a partial quenching of the orbital part of the hyperfine interaction [34]. However, we may propose that at the temperature decreasing below 2 K, phosphorus donors will begin to reorient and they can be observed in the EPR spectrum.

Neither isotropic nor anisotropic hyperfine splitting in echo-detected EPR spectra of phosphorus related centers at temperature of 5 K in the P-doped diamond plates with (111), (110), and (001) surface orientations were detected. This is consistent with the fact that the wave functions on phosphorus for the $1s(T_2)$ or $1s(B_2)$ donor ground states in T_d or D_{2d} symmetries have a predominant p-character with a node at the donor nucleus ($|\Psi(0)|^2 = 0$), when no isotropic hyperfine interaction should be observed [44,45].

Let us consider alternative interpretations of the splitting of 1.05 meV observed in the high-resolution infrared absorption spectra of the high-quality P-doped single crystal diamonds.

First, the 1.05-meV splitting of the T_2 donor ground state in T_d symmetry can be caused by random lattice deformation. However, for example, such splitting in silicon with lithium shallow donor center is much less and equal to ~2 μeV (~0.016 cm^{-1}) [30]. Random lattice strain is also

responsible for the deformation level splitting of ~0.04 cm^{-1} observed in the high-resolution IR absorption spectra of the $LiYF^4:Tm^{3+}$ and $^7LiYF^4:Ho^{3+}$ single crystals with Tm^{3+} and Ho^{3+} concentrations of ~0.1 at.% respectively [71,72]. Thus, we cannot explain the 1.05 meV energy level splitting of the T_2 donor ground state due to the very large difference between the deformation levels splitting in the range from ~0.01 to 0.04 cm^{-1} and that of 8.5 cm^{-1} measured experimentally. Moreover, such the small values of the random crystal lattice strain can be associated with a partial quenching by the orbital strain operator at the dynamic JT vibronic coupling, known as Ham reduction factor [34]. It is also worth noting that we investigated many diamond single crystals with phosphorus concentrations differing by orders of magnitude, and even CVD films, and everywhere we observed the same ground-state splitting of ~1 meV.

Second, another direction for the JT distortion with C_{3v} symmetry can be considered. In this case, the static trigonal JT distortion will split the triply degenerate $1s(T_2)$ state in the T_d configuration into the nondegenerate $1s(A_1)$ ground state, and the doubly degenerate $1s(E)$ state in the C_{3v} configuration, similarly to the substitutional nitrogen atom. The JT energy for the substitutional P measured either as the reduction in total energy or by the splitting of the $1s(T_2)$ level of the on-site defect into $1s(A_1)$ and $1s(E)$ levels with energy between them up to ~100 meV [27]. Only the symmetric A_1 donor ground state has the nonzero square of the absolute value of the wave function $|\Psi(0)|^2$ and only it has a hyperfine interaction with the donor nucleus that is needed to observe the EPR signal. Since we no observe EPR signals related with the P donor, the $1s(B_2)$ state in the D_{2d} configuration is unambiguously the donor ground state of the P-doped diamond.

Third, the splitting of the excited states can be proposed. We definitely observe the splitting of the $1s(T_2)$ donor ground state in the T_d configuration, which is confirmed by the same value of the splitting for all $1s(B_2, E) \rightarrow np_0, np_\pm$ donor transitions from the ground to excited states and by the temperature behavior of the doublet IR bands of donor transitions in agreement with the Boltzmann law. The deformation splitting of NV^- centers in diamond was observed [73], which does not show the temperature dependence associated with the population.

Hence, our considerations have sufficed to demonstrate the occurrence of the dynamic JT effect in the P-doped diamond to provide the general form and magnitude of this effect and to give a quantitative analysis of the electronic band structure of the P-doped diamond using this effect.

IV. CONCLUSIONS

In summary, we have studied the electronic band structure of the large-sized, high-quality P-doped single crystal diamonds grown by the HPHT technique using infrared absorption, magneto- and electron paramagnetic resonance spectroscopy and first-principles calculations. The complete picture of the $1s \rightarrow np_\pm$ and $1s \rightarrow np_0$ ($n = 2, 3, 4$) donor transitions with new $1s \rightarrow 3p_0, 4p_0$ and $1s \rightarrow 4p_\pm$ transitions allowed to refine the energy levels of excited states with those obtained from effective mass approximation calculation. The observation of the $1s \rightarrow 4p_\pm$ transition at 590 meV indicates that the position of the donor ground level is at least 595 meV. For the first time, as far as we know, we have observed the fine doublet structures of the $1s(B_2, E) \rightarrow 2p_\pm$, $1s(B_2, E) \rightarrow 4p_0$, $1s(B_2, E) \rightarrow 3p_\pm$, and $1s(B_2, E) \rightarrow 4p_\pm$ donor transitions with the splitting value of 1.05 meV (8.5 cm^{-1}). We attribute the origin of these doublet structures to the dynamic Jahn-Teller distortion splitting the energy level of the $1s(T_2)$ state in the T_d configuration into those of the $1s(B_2)$ ground state and the $1s(E)$ state in the D_{2d} configuration. This attribution to the dynamic JT effect is experimentally proved by the observation of vibronic energy levels, by the temperature behavior of the doublet IR bands of donor transitions in agreement with the Boltzmann law, by the electron population only of the $1s(B_2)$ ground state at the temperature of 2 K, and by the absence of EPR signals related with P-donor since no isotropic hyperfine interaction should be observed for the $1s(B_2)$ ground state having a predominant p character with a node at the donor nucleus [$|\Psi(0)|^2 = 0$]. The small ~0.002 Å displacement of the substitutional P atom from the T_d tetrahedral position to the D_{2d} tetragonal one and several-meV splitting of T_2 level found from DFT calculations also confirm this attribution. We theoretically found the energy levels of 0.60 eV and 0.40, 0.36 eV corresponding to the $1s(T_2)$ ground state and the $1s(E)$, $1s(A_1)$ exited donor states caused by the valley-orbit interaction. The exited $1s(E)$ energy level of 387 meV instead of 400 meV calculated theoretically has been defined as the difference between the 542 meV vibronic energy level observed experimentally and the 155-meV longitudinal optic phonon. Finally, the vibronic energy level of ~517 meV formed due to the dynamic JT coupling of the exited $1s(E)$ electronic energy level equal to 387 meV with the longitudinal acoustic phonon of ~130 meV interacts resonantly with the electronic level of 524 meV observed in the IR absorption spectrum as the $2p_0$ band that results in it dramatic broadening with the full width at half maximum of ~8 meV.

[1] J. Y. Tsao, S. Chowdhury, M. A. Hollis, D. Jena, N. M. Johnson, K. A. Jones, R. J. Kaplar, S. Rajan, C. G. Van de Walle, E. Bellotti, C. L. Chua, R. Collazo, M. E. Coltrin, J. A. Cooper, K. R. Evans, S. Graham, T. A. Grotjohn, E. R. Heller, M. Higashiwaki, M. S. Islam, P. W. Juodawlkis, M. A. Khan, A. D. Koehler, J. H. Leach, U. K. Mishra, R. J. Nemanich, R. C. N. Pilawa-Podgurski, J. B. Shealy, Z. Sitar, M. J. Tadjer, A. F. Witulski, M. Wraback, and J. A. Simmons, Adv. Electron. Mater. **4**, 1600501 (2018).

[2] M. J. Gullans and J. M. Taylor, Phys. Rev. B **92**, 195411 (2015).

[3] K. Saeedi, S. Simmons, J. Z. Salvail, P. Dluhy, H. Riemann, N. V. Abrosimov, P. Becker, H.-J. Pohl, J. J. L. Morton, and M. L. W. Thewalt, Science **342**, 830 (2013).

[4] T. A. Abtew, Y. Y. Sun, B.-C. Shih, P. Dev, S. B. Zhang, and P. Zhang, Phys. Rev. Lett. **107**, 146403 (2011).

[5] K. J. Morse, R. J. S. Abraham, A. DeAbreu, C. Bowness, T. S. Richards, H. Riemann, N. V. Abrosimov, P. Becker, H.-J. Pohl, M. L. W. Thewalt, and S. Simmons, Sci. Adv. **3**, e1700930 (2017).

[6] R. Kalish, Diamond Relat. Mater. **10**, 1749 (2001).

[7] A. T. Collins and A. W. S. Williams, J. Phys. C **4**, 1789 (1971).
[8] S. Koizumi, H. Ozaki, M. Kamo, Y. Sato, and T. Inuzuka, Appl. Phys. Lett. **71**, 1065 (1997).
[9] H. Sternschulte, K. Thonke, R. Sauer, and S. Koizumi, Phys. Rev. B **59**, 12924 (1999).
[10] E. Gheeraert, S. Koizumi, T. Teraji, H. Kanda, and M. Nesladek, Diamond Relat. Mater. **9**, 948 (2000).
[11] M. Nesladek, K. Meykens, K. Haenen, L. M. Stals, T. Teraji, and S. Koizumi, Phys. Rev. B **59**, 14852 (1999).
[12] T. A. Grotjohn, D. T. Tran, M. K. Yaran, S. N. Demlow, and T. Schuelke, Diamond Relat. Mater. **44**, 129 (2014).
[13] H. Kato, D. Takeuchi, N. Tokuda, H. Umezawa, H. Okushi, and S. Yamasaki, Diamond Relat. Mater. **18**, 782 (2009).
[14] S. N. Polyakov, V. N. Denisov, B. N. Mavrin, A. N. Kirichenko, M. S. Kuznetsov, S. Yu. Martyushov, S. A. Terentiev, and V. D. Blank, Nanosc. Res. Lett. **11**, 11 (2016).
[15] H. Kim, R. Vogelgesang, A. K. Ramdas, S. Rodriguez, M. Grimsditch, and T. R. Anthony, Phys. Rev. Lett. **79**, 1706 (1997).
[16] P. A. Crowther, P. J. Dean, and W. F. Sherman, Phys. Rev. **154**, 772 (1967).
[17] H. Kim, R. Vogelgesang, A. K. Ramdas, S. Rodriguez, M. Grimsditch, and T. R. Anthony, Phys. Rev. B **57**, 15315 (1998).
[18] A. K. Ramdas and S. Rodriguez, Rep. Prog. Phys. **44**, 1297 (1981).
[19] B. Pajot, *Optical Absorption of Impurities and Defects in Semiconducting Crystals* (Springer-Verlag, Berlin, 2010).
[20] C. Jagannath, Z. W. Grabowski, and A. K. Ramdas, Phys. Rev. B **23**, 2082 (1981).
[21] K. Jackson, M. R. Pederson, and J. G. Harrison, Phys. Rev. B **41**, 12641 (1990).
[22] E. B. Lombardi, A. Mainwood, and K. Osuch, Phys. Rev. B **70**, 205201 (2004).
[23] H. Y. Yu, N. Gao, H. D. Li, X. R. Huang, and T. Cui, Chin. Phys. Lett. **36**, 116101 (2019).
[24] T. Nishimatsu, H. Katayama-Yoshida, and N. Orita, Physica B **302-303**, 149 (2001).
[25] L. G. Wang and A. Zunger, Phys. Rev. B **66**, 161202(R) (2002).
[26] S. J. Sque, R. J. Jones, J. P. Goss, and P. R. Briddon, Phys. Rev. Lett. **92**, 017402 (2004).
[27] J. Eyre, J. P. Goss, P. R. Briddon, and J. P. Hagon, J. Phys.:Condens. Matter **17**, 5831 (2005).
[28] B. Butorac and A. Mainwood, Phys. Rev. B **78**, 235204 (2008).
[29] R. L. Aggarwal, P. Fisher, V. Mourzine, and A. K. Ramdas, Phys. Rev. **138**, A882 (1965).
[30] G. D. Watkins and F. S. Ham, Phys. Rev. B **1**, 4071 (1970).
[31] W. V. Smith, P. P. Sorokin, I. L. Gelles, and G. J. Lasher, Phys. Rev. **115**, 1546 (1959).
[32] J. H. N. Loubser and J. A. van Wyk, Rep. Prog. Phys. **41**, 1201 (1978).
[33] R. J. Cook and D. H. Whiffen, Proc. R. Soc. Lond. A **295**, 99 (1966).
[34] F. S. Ham, Phys. Rev. **138**, A1727 (1965).
[35] G. Davies, Rep. Prog. Phys. **44**, 787 (1981).
[36] E. Gheeraert, S. Koizumi, T. Teraji, and H. Kanda, Solid State Commun. **113**, 577 (2000).
[37] E. Gheeraert, N. Casanova, S. Koizumi, T. Teraji, and H. Kanda, Diamond Relat. Mater. **10**, 444 (2001).
[38] E. Gheeraert, N. Casanova, A. Tajani, A. Deneuville, E. Bustarret, J. A. Garrido, C. E. Nebel, and M. Stutzmann, Diamond Relat. Mater. **11**, 289 (2002).
[39] N. Casanova, A. Tajani, E. Gheeraert, E. Bustarret, J. A. Garrido, C. E. Nebel, and M. Stutzmann, Diamond Relat. Mater. **11**, 328 (2002).
[40] I. Stenger, M. A. Pinault-Thaury, A. Lusson, T. Kociniewski, F. Jonard, J. Chevalier, and J. Barjon, Diamond Relat. Mater. **74**, 24 (2017).
[41] K. Haenen, K. Meykens, M. Nesladek, G. Knuyt, L. M. Stals, T. Teraji, and S. Koizumi, Phys. Stat. Sol. a **181**, 11 (2000).
[42] K. Haenen, M. Nesládek, L. De Schepper, R. Kravets, M. Vaněček, S. Koizumi, Diamond Relat. Mater. **13**, 2041 (2004).
[43] N. Casanova, E. Gheeraert, E. Bustarret, S. Koizumi, A. Teraji, H. Kanda, and J. Zeman, Phys. Status Solidi A **186**, 291 (2001).
[44] T. D. Castner, Phys. Rev. **155**, 816 (1967).
[45] J. Isoya, M. Katagiri, T. Umeda, S. Koizumi, H. Kanda, N. T. Son, A. Henry, A. Gali, and E. Janzén, Physica B **376-377**, 358 (2006).
[46] G. Feher, Phys. Rev. **114**, 1219 (1959).
[47] N. D. Samsonenko, V. V. Tokii, and S. V. Gorban, Sov. Phys. Solid State **33**, 1409 (1991).
[48] J. Isoya, H. Kanda, M. Akaishi, Y. Morita, and T. Ohshima, Diamond Relat. Mater. **6**, 356 (1997).
[49] T. Graf, M. S. Brandt, C. E. Nebel, M. Stutzmann, and S. Koizumi, Phys. Status Solidi A **193**, 434 (2002).
[50] M. Katagiri, J. Isoya, S. Koizumi, and H. Kanda, Phys. Status Solidi A **201**, 2451 (2004).
[51] N. Casanova, E. Gheeraert, A. Deneuville, C. Uzan-Saguy, and R. Kalish, Diamond Relat. Mater. **10**, 580 (2001).
[52] M. E. Zvanut, W. E. Carlos, J. A. Freitas, Jr., K. D. Jamison, and R. P. Hellmer, Appl. Phys. Lett. **65**, 2287 (1994).
[53] V. A. Nadolinny, Yu. N. Pal'yanov, A. A. Kalinin, I. N. Kupriyanov, S. L. Veber, and M. J. Newton, Appl. Magn. Reson. **41**, 371 (2011).
[54] S. A. Kajihara, A. Antonelli, J. Bernholc, and R. Car, Phys. Rev. Lett. **66**, 2010 (1991).
[55] J. P. Goss, R. Jones, M. I. Heggie, C. P. Ewels, P. R. Briddon, and S. Oberg, Phys. Rev. B **65**, 115207 (2002).
[56] B. Sadigh, T. J. Lenosky, M.-J. Caturla, A. A. Quong, L. X. Benedict, T. D. De La Rubia, M. M. Giles, M. Foad, C. D. Spataru, and S. G. Louie, Appl. Phys. Lett. **80**, 4738 (2002).
[57] M. Akaishi, H. Kanda, and S. Yamaoka, Science **259**, 1592 (1993).
[58] Yu. N. Palyanov, I. N. Kupriyanov, A. G. Sokol, A. F. Khokhryakov, and Yu. M. Borzdov, Cryst. Growth Des. **11**, 2599 (2011).
[59] D. Saada, J. Adler, and R. Kalish, Appl. Phys. Lett. **77**, 878 (2000).
[60] P. Goss, P. R. Briddon, R. Jones, and S. Sque, Diamond Relat. Mater. **13**, 684 (2004).
[61] G. Alfieri, L. Kranz, and A. Mihaila, Phys. Stat. Sol. RRL **12**, 1700409 (2018).
[62] A. S. Bernard, S. P. Russo, and I. K. Snook, Philos. Mag. **83**, 1163 (2003).
[63] R. Dovesi, R. Orlando, A. Erba, C. M. Zicovich-Wilson, B. Civalleri, S. Casassa, L. Maschio, M. Ferrabone, M. De La Pierre, P. D'Arco, Y. Noel, M. Causa, and M. Rerat, and B. Kirtman, Int. J. Quantum Chem. **114**, 1287 (2014).

[64] J. Heyd, G. E. Scuseria, and M. Ernzerhof, J. Chem. Phys. **118**, 8207 (2003).
[65] K. E. Spear, A. W. Phelps, and B. White, J. Mater. Res. **5**, 2277 (1990).
[66] M. Rohlfing, P. Kruger, and J. Pollmann, Phys. Rev. B **48**, 17791 (1993).
[67] M. R. Salehpour and S. Satpathy, Phys. Rev. B **41**, 3048 (1990).
[68] J. L. Warren, J. L. Yarnell, G. Dolling, and R. A. Cowley, Phys. Rev. **158**, 805 (1967).
[69] S. A. Solin and A. K. Ramdas, Phys. Rev. B **1**, 1687 (1970).
[70] A. Onton, P. Fisher, and A. K. Ramdas, Phys. Rev. Lett. **19**, 781 (1967).
[71] S. A. Klimin, D. S. Pytalev, M. N. Popova, B. Z. Malkin, M. V. Vanyunin, and S. L. Korableva, Phys. Rev. B **81**, 045113 (2010).
[72] K. N. Boldyrev, M. N. Popova, B. Z. Malkin, and N. M. Abishev, Phys. Rev. B **99**, 041105(R) (2019).
[73] T. B. Biktagirov, A. N. Smirnov, V. Yu. Davydov, M. W. Doherty, A. Alkauskas, B. C. Gibson, and V. A. Soltamov, Phys. Rev. B **96**, 075205 (2017).